science, engineering and health studies

Research Article

Science, Engineering and Health Studies
https://lio1.tci-thaijo.org/index.php/sehs
ISSN (Online): 2630-0087

A fabrication of cost-effective paper-based colorimetric devices for nitrite detection

Chanika Pinyorospathum[1], Jeerapat Choeychit[2], Parima Tiawpisitpong[2] and Kanokwan Charoenkitamorn[2]*

[1] National Laboratory Animal Center of Mahidol University (NLAC−MU), Nakhon Pathom 73170, Thailand
[2] Department of Chemistry, Faculty of Science, Silpakorn University, Nakhon Pathom 73000, Thailand

***Corresponding author**: Kanokwan Charoenkitamorn charoenkitamorn_k@su.ac.th*

***Received**: 28 October 2022*
***Revised**: 7 December 2022*
***Accepted**: 8 December 2022*
***Published**: 29 December 2022*

***Citation**: Pinyorospathum, C., Choeychit, J., Tiawpisitpong, P., and Charoenkitamorn, K. (2022). A fabrication of cost-effective paper-based colorimetric devices for nitrite detection. Science, Engineering and Health Studies, 16, 22020013.*

ABSTRACT

Ubiquitous and cost−effective printing paper was remodeled into a colorimetric paper−based analytical devices (PADs) for nitrite anion (NO_2^-) detection via Mn^{7+} reduction in acidic conditions for food and environmental samples. The colorimetric PADs fabricated by wax printing required only 10 µL of potassium permanganate ($KMnO_4$) and to detect NO_2^-. Colorimetry allowed simple visual detection with the naked eye. Image analysis of photographic results revealed the improved detection limit of 0.13 mg/L. Under optimized parameters, including $KMnO_4$ and sulfuric acid (H_2SO_4) concentrations, and reaction time, it was found that colorimetric data were in a logarithmic relationship with the NO_2^- amount ranging from 0.50 mg/L to 5.0 mg/L. Moreover, the colorimetric PADs showed a good selectivity toward NO_2^- among other anions at 100−fold. Application in NO_2^- detection in meat, animal feed, soil, and water samples using the standard addition method revealed 99.7% accuracy for PADs. The proposed technique was validated by traditional spectrophotometry, and a precision in the range of 95.2% to 104.6% was obtained. Therefore, inexpensive, portable, and feasible colorimetric PADs for NO_2^- were successfully constructed.

Keywords: nitrite; potassium permanganate; paper−based analytical devices; food samples; environmental samples

1. INTRODUCTION

Nitrite anions (NO_2^-) are metastable intermediates formed during nitrification and denitrification in the environment and naturally exist in soil, water, and agricultural products. NO_2^- also appears in living tissues because of nitrogen metabolism (van Faassen et al., 2007). Owing to its explicit ability to interrupt the growth of *Clostridium botulinum*, NO_2^- was applied as a food preservative. It also gives meat a presentable red color and odor, and it currently can not be replaced by any substitutes (Feiner, 2016). However, prolonged NO_2^- ingestion is related to methemoglobinemia, a condition where the blood becomes incapable of oxygen transportation due to ferric ion oxidation (Tomasso, 1997). The World Health Organization (WHO) warned of a connection between nitrosamine, a potential carcinogen, and NO_2^- (WHO, 2019). Given these issues, the WHO declares that NO_2^- level must be regulated depending on the region, such as below 0.2 mg/L in drinking water, below 0.5 mg/L in European Union, and below 0.05 mg/L in Japan (Abdollahi and Khaksar, 2014). NO_2^- is widely occurring not only in water, the European Food Safety Authority suggests the acceptable daily intake at 3.7 mg/L body weight (Massey, 1997).

Three methods are currently used for NO_2^- detection. Potentiometry using solid−contact solvent polymeric

membrane ion–selective electrodes (ISEs) has been used. Metalloporphyrin membranes, such as bromo(pyridine) (5,10,15,20–tetraphenylporphyrlnato) cobaltate(CoTPP(py)Br), have been employed as selective ionophores for NO_2^- (Li and Harrison, 1991). These compounds allow ions to transfer across the membrane, and the resulting voltage differences are then measured. (CoTPP(py)Br) developed in a polyvinyl chloride–based membrane has a logarithmic relationship with analytical signal in NO_2^- concentration from 10^{-1} M to 10^{-5} M. Unfortunately, ISEs depend on pH and require frequent calibration due to signal drift. Although these issues have been corrected in commercially available ISEs, the electrode still requires overnight pre–conditioning to prevent nitrite oxidation. In addition, the sensitivity is poor in the presence of F^-, Cl^-, NO_3^-, and SO_4^{2-}. Another electrochemical technique for NO_2^- detection is coupled contactless conductivity detection (C^4D) (Freitas et al., 2016). This device directly measures the conductivity from ions regardless of species and thus requires coupling with a separation technique using anion exchange resin, such as quaternary ammonium salts ($-N^+(CH_3)OH^-$)(Samatya et al., 2006). Even though the system can be miniaturized, but it is not available for on–site analysis due to high maintenance costs, including the expense for the pump and column. Lastly, optical detection is another approach for NO_2^- detection and involves the Griess reaction reagent. In this reaction, NO_2^- reacts with an aniline derivative to form a diazonium salt, which then reacts with a coupling agent such as N–(1–naphthyl)ethylenediamine to form a pink–red azo compound. The signals are monitored with spectrophotometers, and the limit of detection is usually at μM level, depending on the experimental condition. The reagent is functionalized onto noble–metal nanoparticles to obtain a selectivity chromophore for NO_2^- detection (Daniel et al., 2009), as a result, the optical properties of the nanoparticles, namely, aggregation or anti–aggregation, are changed. Although the absorption is improved, exposure to the chemicals should be avoided because diamine moieties are a carcinogenic substance (Booth, 2000). Other modifiers, such as *p*–aminothiophenol (Liu et al., 2015) and diethyl 2–amino–6–bromoazulene–1,3–dicarboxylate (azulene) (Murfin et al., 2020) can be used. These nanoparticles have increased analytical performance but easily precipitate under unsuitable dispersing conditions (Li et al., 2008), such as high salt concentration and low pH (Bihari et al., 2008). Therefore, the development of a simple and stable detection method for NO_2^- is necessary.

NO_2^- exhibits reducing activity and can undergo redox reactions with transition metals and change their optical properties. In this type of reaction, NO_2^- can be directly detected in a fast reaction without requiring nanomaterials. Potassium permanganate ($KMnO_4$) is a good candidate because it is a strong oxidizing agent and has purple color due to the formation of ligand–to–metal charge transfer complexes. It is commonly used in a qualitative evaluation technique for redox species (permanganometry), such as iron (Fe^{2+}), oxalate, nitrite, and hydrogen peroxide. The oxidation state +7 of manganese ions could be reduced to +2, +4, or +6, depending on the reaction conditions, and the corresponding colors could also change from colorless, brown, and green, respectively (Murthy, 2008). The redox reaction with NO_2^- occurs favorably at low pH. Mn^{2+} is the dominant product, and the solution is colorless. The color changes are visible to the naked eye and distinct in the absorption spectra. Furthermore, experiments could be designed for analytical detection on various platforms, such as paper (Wang et al., 2015), thread (Singhaphan and Unob, 2021), and capillary (Sieben et al., 2010).

Many analytical methods can be minimized on disposable platforms. Paper–based analytical devices (PADs) are the most popular for point–of–care diagnosis in developing countries (Hasanzadeh and Hashemzadeh, 2021). PADs are an answer to reliable analysis in rural areas where a central laboratory is difficult to access. These devices are affordable and offer easy and fast assays. Paper supports biological and environmental analytes because of its biocompatible nature. On PADs, the analyte solution is carried to several zones via capillary action without external pump (Lam et al., 2017) and can undergo pretreatment, separation, and intermediate formation, depending on the reactions specified in the design. Liquid transportation is limited in the channel by a fabricated device and usually stops for detection at the end. In addition, PADs could be combined with various detection systems, such as Raman, electrochemistry, and colorimetry (Akyazi et al., 2018). Many researchers stated that optimized analytical methods based on PADs resemble bulk techniques with advantages of green chemistry. In general, PADs are fabricated using filter paper, in particular Whatman No.1, because of its strong affinity to water (high absorptivity) and suitability for filtration, retention (in paper chromatography), and flow analysis (for PAD application). Although some researchers attempted to introduce new features into paper, such as superhydrophobic properties (Wang et al., 2016), only a few employed affordable and accessible printing paper. Herein, NO_2^- detection based on a redox reaction with $KMnO_4$ using PADs made from printing paper was proposed for the first time. The colorimetric results were measured qualitatively and quantitatively on PADs. The effects of relevant parameters were studied and optimized. The proposed technique was applied to NO_2^- determination in actual food and environmental samples, and the recovery was compared with that using conventional Griess reaction reagent.

2. MATERIALS AND METHODS

2.1 Chemicals and reagents

All chemicals of analytical grade were purchased from Sigma–Aldrich (St. Louis, MO, United States) and stored at recommended conditions throughout the study. Sodium nitrite ($NaNO_2$) and $KMnO_4$ were obtained from KemAus (New South Wales, Australia). Sulfuric acid (H_2SO_4) and Griess reagent were traded from Carlo Erba reagents (Lombardia, Italy) and Sigma–Aldrich (St. Louis, MO, USA), respectively. Distilled water was acquired from Thermo Fisher Scientific (18.2 mΩ cm, Massachusetts, USA).

Meat samples, including sausages, salami, and pork mince were purchased from the local market in Nakhon Pathom, Thailand. Rodent and rabbit feeds were sampled from the feed storage of the National Laboratory Animal Center, Mahidol University (NLAC–MU). Dog food was bought from a department store. Soil and water were collected from a farming area within NLAC–MU. Food and soil samples were crushed and extracted in water at 30°C and 80 rpm for 1.5 h. Afterward, the supernatant was filtered with nylon membrane to remove any remaining suspensions. The water samples were used as received.

2.2 Instruments

Photographs were captured using a smartphone camera (iPhone 6). ISO and white balance were controlled at 1000 and 6000, respectively. A cubic lightbox of 30 cm dimension was used to fix the light condition. A mean intensity was analyzed with ImageJ (NIH, USA). UV–visible absorption was recorded using a double–beam spectrophotometer UV–1900i purchased from Shimadzu (Kyoto, Japan). The material of cuvette was quartz with 10.0 mm pathlength.

2.3 Fabrication of colorimetric PADs

Patterns were a symmetrical, circular shape of 5.0 mm diameter drawn in Microsoft PowerPoint. Wax printing was adopted to fabricate the colorimetric PADs. Design patterns were printed with a Xerox ColorQube printer (Connecticut, USA) onto A4 paper (Double–A Holdings Limited, Thailand), then cut into approximately 10 × 10 items, and placed on a hot plate at 180°C for 1 min. The pattern should be clearly seen from both sides; otherwise, the paper was continuously heated for additional seconds. Finally, the device was taped at one side to stop leakage. The fabrication of the device is depicted in Figure 1. Deionized water was filled and dried at room temperature to improve the hydrophilicity of the office paper before use.

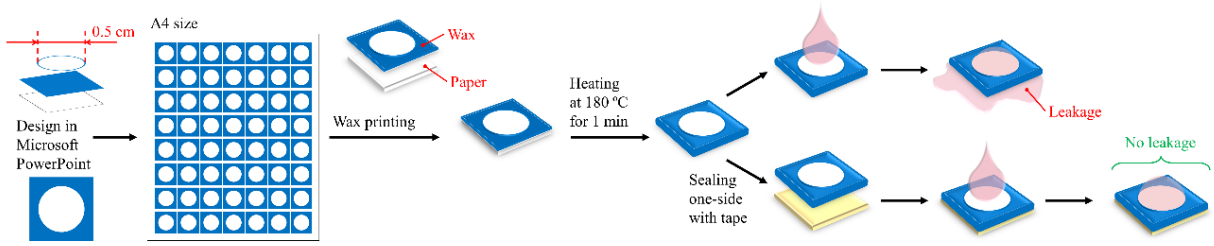

Figure 1. Fabrication process of colorimetric PADs using wax printing method

2.4 NO_2^- detection on colorimetric PADs

The chemicals were consecutively dropped onto colorimetric PADs. First, 10.0 µL of acid solution was added, followed by equivalent volumes of $KMnO_4$ and then analyte ions or cat/anions. The pink solution of $KMnO_4$ was decolorized by analyte ions, and this process could be visualized by the naked eye. For image post–processing, photos of the devices were taken and analyzed with ImageJ. Numerical results were represented by Δ mean intensity of the RGB color model, which is the subtraction of the value at the measuring point by the blank's signal. The data was further calculated to obtain semi–quantitative data. Chemicals' concentration, reaction time, and image channels (red, green, and blue) were studied. The experiments were carried out in parallel with UV–visible spectrophotometry using a commercial test kit of Griess reagent. All measurements were performed at least in triplicate.

3. RESULTS AND DISCUSSION

3.1 UV–visible measurement of $KMnO_4$ colorimetric reaction

In this work, MnO_4^- was used to oxidize NO_2^- to NO_3^-. The pink color of $KMnO_4$ diminished depending on the amount of NO_2^- presented in the solution. Decolorization occurred because Mn^{7+} was reduced to Mn_2^+. The redox reaction could be written as follow:

$$2MnO_4^- + 5NO_2^- + 6H^+ \rightarrow 2Mn^{2+} + 5NO_3^- + 3H_2O \qquad (1)$$

Different combinations of NO_2^-, $KMnO_4$, and H_2SO_4 were investigated using UV–visible spectra, and the results are depicted in Figure 2A. NO_2^- alone showed a large absorption at 209, along with a trivial absorption at 361 nm. Similar to H_2O, H_2SO_4 had no absorption peak. $KMnO_4$ had two absorptions around 317 and 525 nm and a small peak at 230 nm. The absorption around 525 nm consisted of multiple spikes (489, 507, 525, 545, and 566 nm) attributed to vibronic transitions. The lower band at 317 nm was assigned to $3t_2 \rightarrow 2e$, and the region around 489-566 nm possibly belonged to $t_1 \rightarrow 2e$ orbital transition (Heit et al., 2019; Hu et al., 2016). Therefore, the absorption spectrum was characteristic of Mn^{7+}. A photograph of the solutions with different compositions is shown in inset a of Figure 2A.

In the presence of NO_2^- and H_2SO_4 (Figure 2B, a peak appeared around 350 nm and was attributed to HNO_2 (Morakinyo et al., 2012). The mixture of $KMnO_4$ and H_2SO_4 showed similar absorption to $KMnO_4$ alone, even when left to react for 1.5 h. In contrast, the mixture of $KMnO_4$ and NO_2^- without H_2SO_4 showed an increment of the baseline ranging from 250 to 450 nm for the spectra recorded every other 0.5 h. After the baselines were corrected by 0 min, the absorbance was found to increase by 19.9%, 36.6%, and 49.1% for 0.5, 1, and 1.5 h, respectively, indicating that the electron transfer was promoted. These results were in agreement with another work, suggesting that the baseline increased because of MnO_2 (Fujimoto et al., 2001). In addition, the mixture (Figure 2B, inset b) was slightly orange in color, which was consistent with a study on the oxidation states of Mn^{4+} (Kolb, 1988). The changed absorbance and color could be related to NO_2^- concentration; however, this mixture is not suitable for rapid detection because the reaction took at least 1.5 h to complete.

Finally, NO_2^- and $KMnO_4$ were studied in H_2SO_4. Figure 2C shows that the absorbance of Mn^{7+}decreased significantly. Even though it also exhibited a time-dependent trend, the absorbance remained stable after 5 min (Figure 2C, inset c). Further experiments with various amounts of the analyte ions were carried out. The results showed that the absorbance decreased analogously with the increasing NO_2^- concentration (Figure 2D). Therefore, the colorimetric assay between $KMnO_4$ and NO_2^- in acidic conditions could be used for the quantification of NO_2^-.

In colorimetric theory, color is perceived by the human eye as the reflective light (wavelength) from the object. Mn^{7+}, which has empty electrons in d–orbital, exhibits a shift of charge density from its ligand (oxygen's p–orbital) to the metal center (ligand–to–metal charge transfer).

During this process, electromagnetic radiation is absorbed, and then light with an intense color is reflected. Meanwhile, Mn^{2+} does not produce a visible color because of its spin–forbidden transitions because only half of the d–orbital is filled (d^5) (Dowsing et al., 1968). In this work, $KMnO_4$ was considered an excellent chromogenic probe because the color changes were highly distinguishable after NO_2^- reduced Mn^{7+} to Mn^{2+} in the acidic environment. Color tones also varied with the remnants of $KMnO_4$ in the solution after reacting with NO_2^-, and these variations were proportional to NO_2^-, concentration (Figure 2, inset d and e). Moreover, MnO_4^- possesses remarkably high molar absorptivity that is ideal for a redox indicator (Morbioli et al., 2017). On the basis of color observations and UV–visible characterization, NO_2^- detection method based on the colorimetric reaction of $KMnO_4$ was developed.

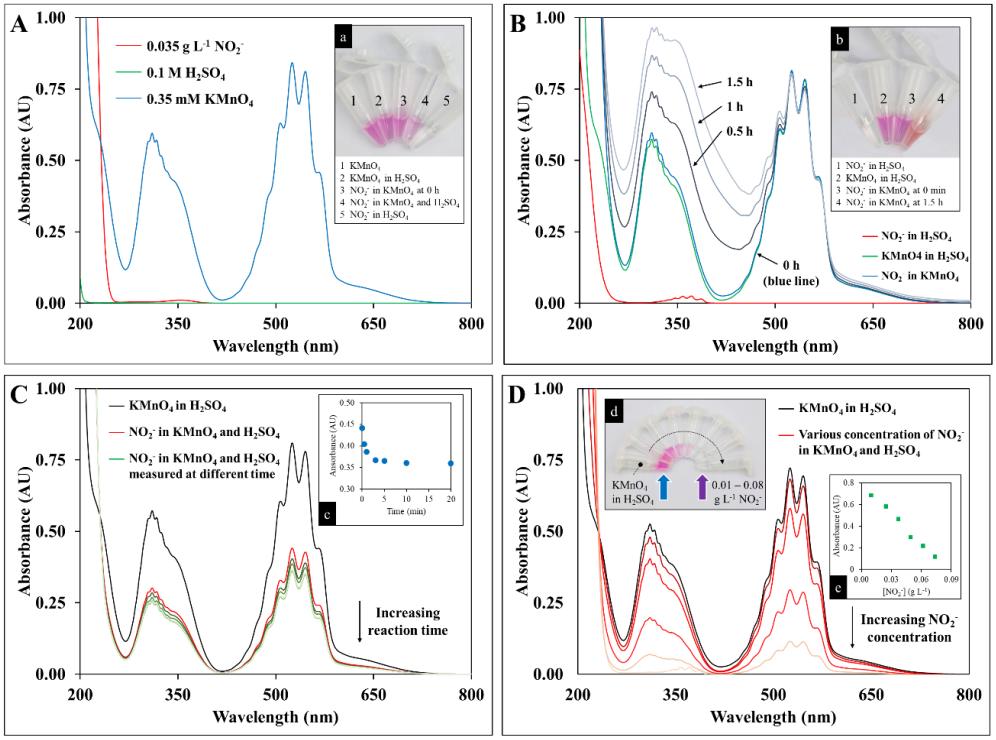

Figure 2. UV–visible characterization of NO_2^- detection based on reaction with MnO_4^-: (A) individual chemical presented in the solution, (B) each pair of different chemicals, (C) all chemicals at various reaction time, and (D) different concentration of NO_2^- in $KMnO_4$ and H_2SO_4

Note: Insets are photographs of (a) different combinations of chemicals (a), (b) taken after 1.5 h (c), a plot between absorbance of $KMnO_4^-$ and reaction time, (d) a photograph of pink shades derived from $KMnO_4$ decolorization by NO_2^- ranging from 0.01 – 0.08 g/L. All reactions were studied under the identical conditions: 0.035 g/L NO_2^- except for (D), 0.1 M H_2SO_4, 0.35 mM $KMnO_4$, and 30-s reaction time except for (B) and (C)

3.2 Effect of pH

NO_2^- could undergo oxidation by MnO_4^- via different pathways. In this colorimetric assay, NO_2^- was designed to react with Mn^{7+} to form Mn^{2+}. The decolorization of the reaction was crucial for the quantification. According to the overall reaction, H^+ involved. Therefore, further experiments were carried out to study the pH dependence of the reaction. The detection system was prepared in the pH range 1 – 13 and monitored using UV–visible spectrophotometry. The selected pH was observed for the reaction as a function of time. The previous characterization revealed the absorption behavior of the system in 0.1 M H_2SO_4 (pH 1). Therefore, the discussion was continued at pH above 1.

The absorption band of pH 3 (Figure 3A) was initially similar to that of pH 1 when measurement was immediately conducted after the NO_2^- addition. During the measurement, the band completely changed with time at 1-10 min. First, the absorption decreased due to the reduction of Mn^{7+} to Mn^{2+}. In the following 5 min, the baseline was lifted, which was close to the behavior of the NO_2^- and $KMnO_4$ mixture without the acid. However, the subtracted baseline yielded similar absorbance to the initial value. A possible reason was that Mn^{2+} and MnO_2 were presented in the solution. In this case, MnO_2 might be derived from the excess NO_2^- and $KMnO_4$ after the hydrogen ions were depleted. With the additional 5 min, the baseline was subdued at almost every absorption peak, but the unique feature spikes at 505, 524, and 544 nm of $KMnO_4$ were retained. The pink solution gradually turned brown (Figure 3B), and particles could be seen with the naked eye. The light scattering by particles was suspected to cause the baseline alleviation (Porterfield and Zlotnick, 2010; Van Eerdenbrugh et al., 2011). These results also corresponded with studies of MnO_2 nanomaterial synthesis (Jaganyi et al., 2013; Kim et al., 2016). Although the findings at pH 3 were informative, the execution of the reaction according to the experimental design had failed.

The solutions at pH 5 and 7 showed identical orange color at 5 min (Figure 3B), although the absorption spectra in Figure 3C revealed that the bands in 317 nm had lower absorbance at pH 5 than at pH 7. The behavior of the absorbance pattern was similar to that in pH 3, in which

MnO_2 was formed but the absorption remained constant after 5 min. Following the designed condition, NO_2^- was first protonated to HNO_2, and active species of nitrogen such as NO^+, N_2O_3, and N_3O_3, were then formed and reacted with MnO_4^-, which later led to the production of NO_3^- and Mn^{2+} (Turney and Wright, 1959). The pK_a of nitrous acid is 3.3 at 25°C (Chenier, 2002), which is lower than that obtained at pH 5. Hence, the reduction of MnO_4^- was less likely to occur. The absorption of pH 7 in Figure 3D was similar to that in Figure 2B and Figure 3C, but the peaks at 317 nm were trivial, compared with those in pH 3 and 5. As explained previously, HNO_2 existed in small amounts due to the pK_a of the solution. Thus, the amount of reactant was insufficient to drive MnO_4^- reduction. Further investigations in basic solutions (pH 9-13) revealed that the addition of NO_2^- did not change the absorbance, and the baselines were not escalated with time, as shown in Figures 3E-F. This finding implied that MnO_4^- was not reduced by NO_2^- in basic condition, and MnO_2 was not generated. Owing to the inappropriate conditions reasoned above, the colorimetric assay in this work was performed below pH 1.

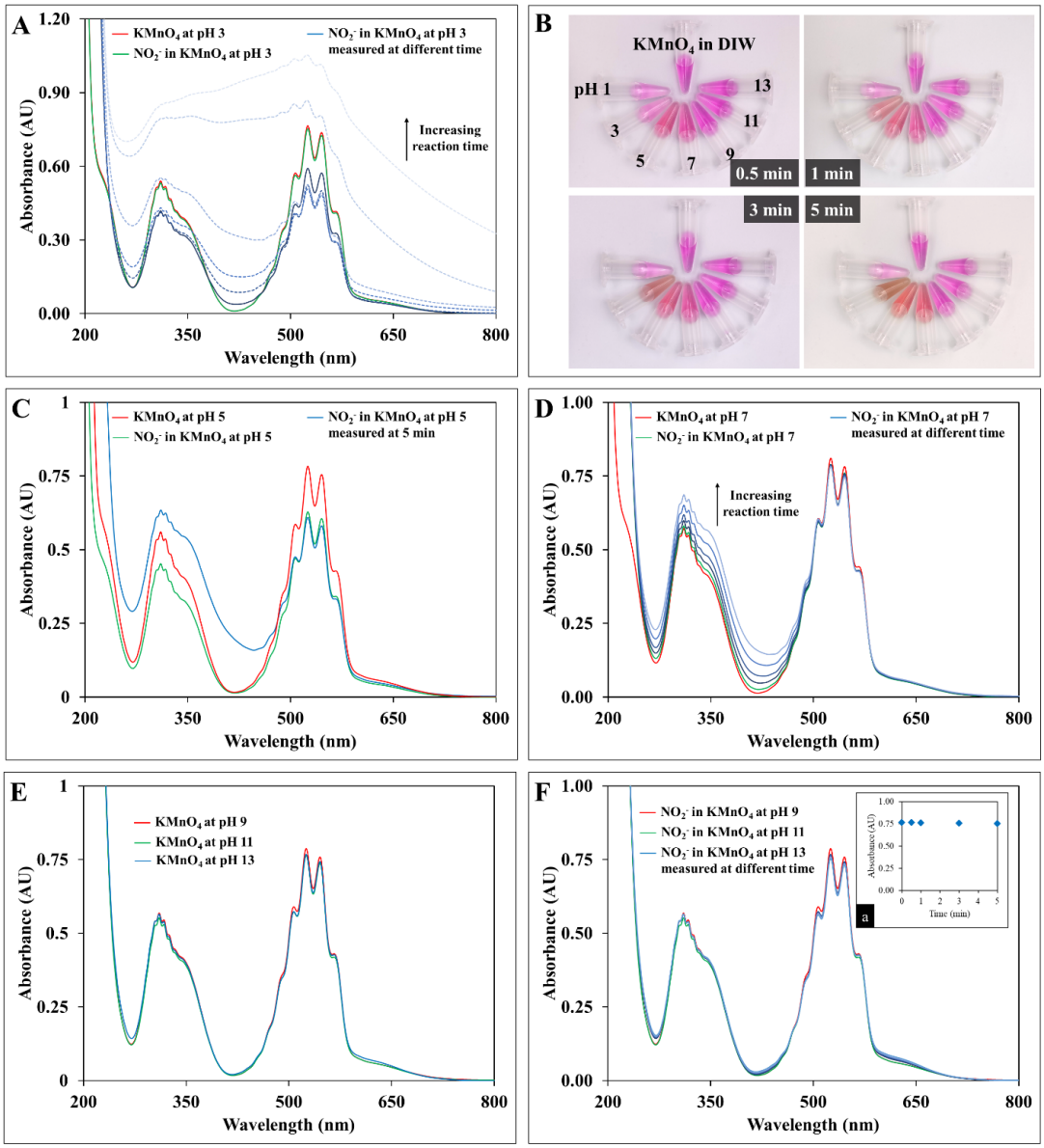

Figure 3. Effect of pH on the proposed detection system: (A) pH 3, photographs of solution consisted of NO_2^- in $KMnO_4$ at (B) different pH ranging from 1 – 13 taken after incubation up to 5 min, (C)pH 5, (D)pH 7, (E) $KMnO_4$ in basic conditions, and (F)addition of NO_2^- into $KMnO_4$ at basic conditions.

Note: Inset (a) is a plot between absorbance and reaction time of pH 13. All reactions were studied under the identical conditions: 0.035 g/L NO_2^-, 0.35 mM $KMnO_4$, while concentration of H_2SO_4 was varied according to pH. pH 3, 7, and 13 at different time (0-10 min) were monitored to observe relationship between absorbance and time as a representative in acid, neutral, and basic solutions, respectively.

3.3 Improving the sensitivity of NO_2^- colorimetric assay on colorimetric PADs

Colorimetric PADs were fabricated for NO_2^- detection using the reaction with MnO_4^-. In addition to the UV–visible investigation, optimization studies were performed on colorimetric PADs to acquire the best sensitivity for the colorimetric approach. The obtained suitable conditions for the system were 5.0 mM $KMnO_4$, 0.6 M H_2SO_4, and three min of reaction time.

3.4 Analytical performance

Various concentrations within 5.0×10^{-6} - 5.0 g/L were studied under the optimized conditions, but only results for 5.0×10^{-2} - 5.0 g/L (0.50 mg/L - 5.0 g/L) were attained. The photographs of the results are displayed in Figure 4A. The mean intensity obtained at each point was nullified by blank subtraction to ensure lighting and color correction. The initial plot between NO_2^- concentration and Δ mean intensity (inset a) showed that a curve was approaching a constant, implying that additional data treatment was required. Therefore, NO_2^- concentration and Δ mean intensity were rearranged in the logarithmic model. The linear relationship was eventually disclosed in Figure 4B for the quantitative determination of NO_2^-. The coefficient of determination (R^2) equaled 0.9995, and the slope was 11.081 L/mg. Limit of detection (LoD) was calculated as 3 × standard deviation (inset b) and divided by slope (3SD/slope), and limit of quantification (LoQ) was computed using 10SD/slope. The values for LoD and LoQ were 0.13 and 0.43 mg/L, respectively. Concentrations at LoD and LoQ were tested on the colorimetric PADs, but the results were unremarkable from the previous experiment. Analogous naked–eye observation at the lighting conditions could initially distinguish the color of the analyte from the blank at 1.0 mg/L; nevertheless, the difference could not be perceived from the photographic result in Figure 4A. Even though the naked–eye observation of NO_2^- using the developed approach is already suitable to determine the acceptable daily intake, combining the proposed method with image processing can improve the detection of NO_2^- concentration limited by EU.

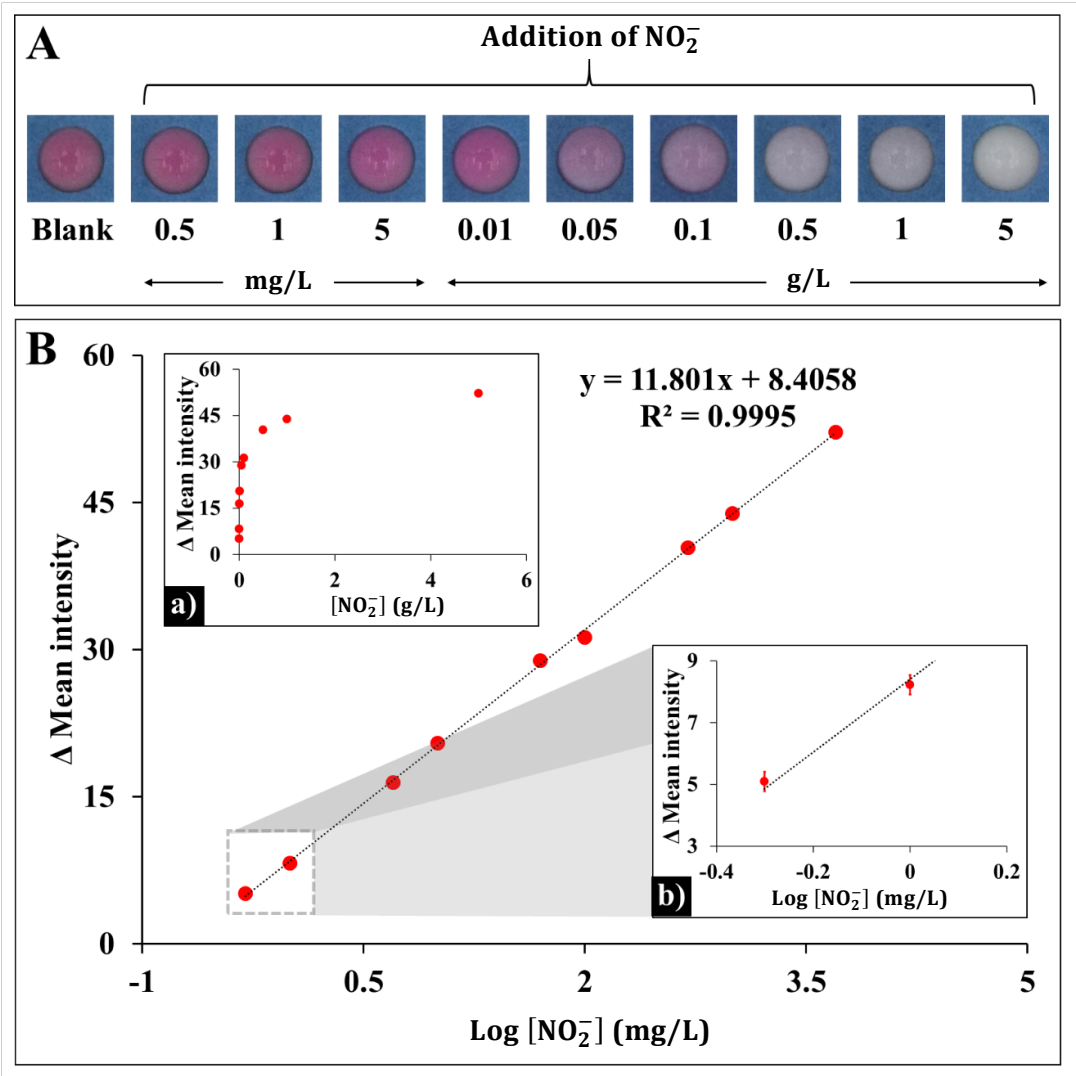

Figure 4. (A) Photographic results of colorimetric PADs after addition of increasing amount of NO_2^- (0.50 mg/L - 5.0 g/L) in 5.0 mM $KMnO_4$ and 0.6 M H_2SO_4, and (B) linear dynamic plot between log $[NO_2^-]$ and Δ mean intensity of blue channel.
Note: Inset (a) calibration plot between NO_2^- concentration and Δ mean intensity value, and (b) magnification plot of 0.50 to 1.0 mg/L NO_2^-.

3.5 Response of other anions to the optimized device

To demonstrate the practical use of this portable device, the potential anions that expected to be found were studied, including Cl^-, NO_3^-, HCO_3^-, $H_2PO_4^-$, CO_3^{2-}, SO_4^{2-}, HPO_4^{2-}, and PO_4^{3-}, with NO_2^- (tolerance study, Figure 5A) and without NO_2^- (selectivity study, Figure 5B). The study was performed in additional period longer than 10 min. According to the observations, the reaction turned brown, possibly due to MnO_2 formation, which is similar to the previous explanation at pH 3. The anions could also spontaneously reduce MnO_4^-, albeit at an incomparable rate with NO_2^- due to the high reduction potential. Changes in the mean intensity of the anions were not higher than 10% at the tested concentration (100–fold of NO_2^-), compared with the analyte. These results showed no remarkable influence of the anions commonly existing in environmental and food samples. Therefore, the colorimetric method proposed in this study had selectivity toward NO_2^-.

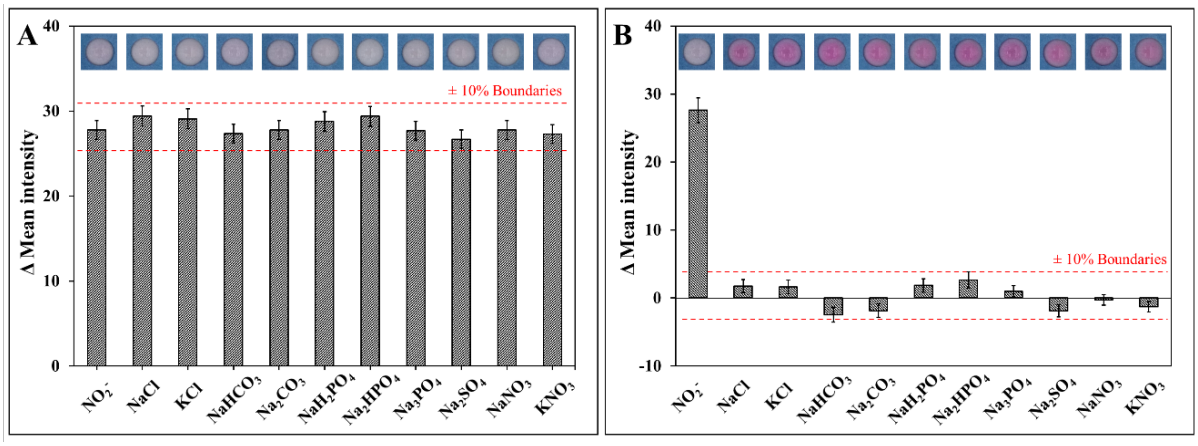

Figure 5. Photographs and the corresponding plots of the mean intensity of (A) tolerance, and (B) selectivity studies
Note: Experimental was performed under the optimal conditions of $KMnO_4$ and H_2SO_4. The reaction time was 3 min. Concentration of NO_2^- and other ions were 0.1 and 10.0 g/L, respectively.

3.6 Method validation in environmental and food samples

The developed colorimetric PADs for NO_2^- detection based on the chemical reduction of $KMnO_4$ was compared with other sensors listed in Table 1 using electrochemical and spectrophotometric measurements. Together with other modifiers, such as carbon nanomaterials (Turdean and Szabo, 2015), enzymes (Almeida et al., 2007), anion exchangers (Li and Harrison, 1991), NO_2^- could be oxidized on the surface of electrodes. The system could enhance the sensitivity and selectivity of the detection. The electrochemical method is usually subjected to electrode fouling, particularly in a miscellaneous matrix. Spectrophotometry, specifically UV–visible outperforms the other techniques and thus is considered as a standard method for the determination of nitrite and nitrate, according to ISO 13395:1996 (ISO, 1996). This guideline suggests the use of a mixture of 0.10 g/L sulfanilamide, 0.010 g/L N–(1–naphthyl)ethylenediamine dihydrochloride, and 0.1% v/v phosphoric acid as a chromogenic agent. In this work, the commercially available Griess reagent was modified for the spectrophotometric analysis of NO_2^-. Apart from the durable instrumentation, UV–visible spectrophotometry offers more reliable results than electrochemistry, and thus was adopted in this study as a validation method for the application of the proposed technique in real sample analysis.

Table 1. Comparison of the methods for NO_2^- determination in food and environmental samples

Methodology	Adaptation	LoD	Real sample	Portable	Reference
Voltammetry	Single-walled carbon nanotubes – myoglobin modified electrode	3.8 mM	Meat	Yes	(Turdean and Szabo, 2015)
Electrochemical - Biosensor	Nitrite redutase/Nafion/methyl viologen	60 µM	–	Yes	(Almeida et al., 2007)
UV-visible	Molybdate	4.0 µg/L	Well, wastewater	No	(Yang and Alleman, 1992)
Colorimetric thread-based platform	Griess reagent	25 µM	Drinking water, Chinese cabbage, and sausage	Yes	(Singhaphan and Unob, 2021)
Colorimetric PADs based on the reaction with MnO_4^-	MnO_4^-	0.13 mg/L	Meats, animal feeds, soils, water	Yes	This work

Samples were collected from specific places described above. The water samples were spiked with NO_2^- without any treatment. The soil and meat samples required extraction prior to the addition of an analyte. Given that both methods could not directly determine NO_2^- from the samples, the standard addition technique was employed. The amount of spiked NO_2^-, measurement values, and recovery percentage between the developed and the validation method were compared and are listed in Table 2. The recovery percentage of NO_2^- on colorimetric PADs was in the range of 95.2% – 104.4% and that of UV–visible spectrophotometry was 96.9% – 105.0%. T–test between the two methods confirmed that the proposed assay on colorimetric PADs was not significantly different from the traditional UV–visible spectrophotometry (t_{stat} (0.8604) < $t_{critical}$ (2.0010)). The accuracy of the colorimetric PADs, which was calculated with respect to the spike concentration of NO_2^-, was equal to 99.7%. The precision derived from 10 replicate measurements at each concentration was within the range of 95.2% to 104.6%. Moreover, the concentration of NO_2^- in real samples could be calculated due to the advantage of the standard addition method used in this work. The content of NO_2^- ranked from the highest to the lowest was as follows: meat (0.5575–2.6330 µg/L), soil (0.0701–0.4680 µg/L), animal feed (0.0749–0.2083 µg/L), and water samples (0.0334–0.1132 µg/L). The results clearly testified that the developed method was feasible for NO_2^- determination in various samples and more beneficial for on–site applications, compared with a standard method. The proposed method also allows for the detection in drinking water samples, according to European standard (a permission level is below 0.5 mg/L) and meat samples according to Ministry of Public Health, Thailand (a permission level is below 80 mg/kg) (Sakolsatayadorn, 2016). Owing to their compelling performance, the colorimetric PADs already overcome the conventional technique in terms of operating cost and portability, especially because this work utilized the platform of printing paper rather than filter paper. The overall price for one analysis session was approximately 0.005 cent (US currency) for the developed colorimetric PADs and 0.2 cent (US currency) for other PADs fabricated with filter paper. Therefore, the proposed colorimetric PADs ultimately surpass the analytical and financial values of other devices.

Table 2. Recovery percentage of NO_2^- in real samples at various spiking concentrations measured with the proposed colorimetric PADs and validated with UV–visible

Samples		Spiked	Colorimetric PADs			UV-visible		
			Found	SD	% Recovery	Found	SD	% Recovery
Meat	Sausages	-	ND	0.0004	-	2.6688	0.0001	-
		1	1.0443	0.0012	104.4	1.0262	0.0002	102.6
		2.5	2.4830	0.0014	99.3	2.5025	0.0011	100.1
		5	4.8430	0.0024	96.9	4.9170	0.0002	98.3
		7.5	7.5750	0.0005	101.0	7.3331	0.0004	97.8
		10	9.6020	0.0024	96.0	9.9500	0.0024	99.5
	Salami	-	ND	0.0005	-	0.5714	0.0000	-
		1	0.9622	0.0027	96.2	1.0061	0.0001	100.6
		2.5	2.5383	0.0026	101.5	2.4658	0.0006	98.6
		5	4.9865	0.0027	99.7	5.0982	0.0008	102.0
		7.5	7.6425	0.0030	101.9	7.5046	0.0003	100.1
		10	9.6790	0.0031	96.8	9.9048	0.0002	99.0
	Pork mince	-	ND	0.0005	-	0.2082	0.0001	-
		1	0.9524	0.0009	95.2	1.0018	0.0001	100.2
		2.5	2.6098	0.0014	104.4	2.5624	0.0001	102.5
		5	5.1320	0.0013	102.6	4.9929	0.0009	99.9
		7.5	7.3598	0.0022	98.1	7.4576	0.0011	99.4
		10	10.3830	0.0013	103.8	10.0006	0.0016	100.0
Animal feed	Rat food	-	ND	0.0001	-	0.0724	0.0000	-
		1	1.0273	0.0027	102.7	1.0493	0.0001	104.9
		2.5	2.4038	0.0050	96.2	2.4341	0.0002	97.4
		5	5.1200	0.0019	102.4	4.8467	0.0002	96.9
		7.5	7.8330	0.0016	104.4	7.4055	0.0002	98.7
		10	9.7980	0.0003	98.0	10.2135	0.0003	102.1
	Dog food	-	ND	0.0003	-	0.2081	0.0000	-
		1	0.9555	0.0011	95.6	1.0501	0.0002	105.0
		2.5	2.5828	0.0011	103.3	2.4399	0.0002	97.6
		5	4.9275	0.0012	98.6	5.1060	0.0003	102.1
		7.5	7.7123	0.0011	102.8	7.4154	0.0012	98.9
		10	10.2360	0.0011	102.4	10.3745	0.0003	103.7

Table 2. Recovery percentage of NO_2^- in real samples at various spiking concentrations measured with the proposed colorimetric PADs and validated with UV–visible (Continued)

Samples		Spiked	Colorimetric PADs			UV-visible		
			Found	SD	% Recovery	Found	SD	% Recovery
Animal feed	Rabbit food	-	ND	0.0007	-	0.1191	0.0000	-
		1	0.9770	0.0033	97.7	0.9858	0.0001	98.6
		2.5	2.5355	0.0032	101.4	2.4666	0.0010	98.7
		5	5.0200	0.0037	100.4	5.1457	0.0001	102.9
		7.5	7.4670	0.0036	99.6	7.6260	0.0002	101.7
		10	9.7080	0.0024	97.1	9.8146	0.0002	98.2
Soil	Sand	-	ND	0.0004	-	0.0688	0.0000	-
		1	0.9728	0.0009	97.2	0.9947	0.0002	99.5
		2.5	2.4495	0.0000	98.0	2.4675	0.0003	98.7
		5	5.0875	0.0004	101.8	5.1545	0.0004	103.1
		7.5	7.3620	0.0048	98.2	7.6187	0.0005	101.6
		10	10.3380	0.0008	103.4	9.8504	0.0005	98.5
	Silt	-	ND	0.0009	-	0.2204	0.0001	-
		1	0.9693	0.0036	96.9	1.0208	0.0001	102.1
		2.5	2.4878	0.0047	99.5	2.5151	0.0002	100.6
		5	5.0245	0.0050	100.5	4.9622	0.0003	99.2
		7.5	7.5015	0.0048	100.0	7.5711	0.0004	101.0
		10	9.9320	0.0044	99.3	9.9485	0.0005	99.5
	Loam	-	ND	0.0008	-	0.4644	0.0000	-
		1	0.9528	0.0029	95.3	1.0155	0.0001	101.6
		2.5	2.5138	0.0027	100.6	2.5592	0.0002	102.4
		5	4.9950	0.0027	99.9	4.8871	0.0004	97.7
		7.5	7.4513	0.0011	99.4	7.4097	0.0005	98.8
		10	9.6270	0.0009	96.3	10.1143	0.0005	101.1
Water	Tap water	-	ND	0.0001	-	0.0331	0.0000	-
		1	0.9595	0.0012	96.0	0.9963	0.0001	99.6
		2.5	2.5988	0.0022	104.0	2.5042	0.0001	100.2
		5	4.9155	0.0032	98.3	4.9118	0.0011	98.2
		7.5	7.2908	0.0048	97.2	7.4005	0.0002	98.7
		10	10.1250	0.0012	101.2	10.1471	0.0003	101.5
	Raw water	-	ND	0.0008	-	0.0671	0.0001	-
		1	1.0340	0.0030	103.4	1.0118	0.0001	101.2
		2.5	2.4110	0.0022	96.4	2.5121	0.0013	100.5
		5	5.1170	0.0014	102.3	4.8908	0.0002	97.8
		7.5	7.3823	0.0001	98.4	7.6496	0.0002	101.2
		10	10.0600	0.0030	100.6	9.9386	0.0031	99.4
	Sewage	-	ND	0.0011	-	0.1102	0.0000	-
		1	1.0143	0.0034	101.4	1.0314	0.0016	103.1
		2	2.4643	0.0018	98.6	2.4748	0.0001	99.0
		3	4.8570	0.0023	97.1	5.0365	0.0002	100.7
		4	7.2458	0.0042	96.6	7.4769	0.0024	99.7
		5	9.7000	0.0062	97.0	9.9970	0.0003	100.0

Note: Values are reported in mg/L, except for non–spiked samples that are calculated to µg/L. ND = not detected.

4. CONCLUSION

Colorimetric NO_2^- detection on colorimetric PADs was developed using $KMnO_4$ as a chromogenic probe. The results showed that typical printing paper could be modified for use in NO_2^- determination, and the colors varied from pink shades to colorless with the increasing concentration of target anions. Mechanism studies using UV–visible spectrophotometry revealed that characteristic absorption between 489 and 566 nm was depleted upon the addition of NO_2^- in acid condition (pH less than 1). The performance of colorimetric PADs depended on acidity, $KMnO_4$ concentration, and reaction time. The maximum efficiency was obtained at 0.6 M H_2SO_4 and 5.0 mM $KMnO_4$. Color changes were captured using smartphone after leaving the reaction for 3 min. Results from image analysis showed that NO_2^- concentration was in a logarithmic relationship with the mean intensity from 0.50 mg/L to 5.0 g/L, and the detection limit was calculated as 0.13 mg/L. Moreover, distinguishable color could be seen as low as 1.0 mg/L. The feasibility of the proposed method for the analysis of meat, animal feed, soil, and water samples was

confirmed with excellent accuracy (99.7%) and precision (95.2% - 104.6%). The colorimetric PADs were modified from printing paper and cost 40 times lower than other PADs fabricated with filter paper.

REFERENCES

Abdollahi, M., and Khaksar, M. R. (2014). Sodium nitrite. In *Encyclopedia of Toxicology* (Wexler, P. ed.), 3rd, pp. 334-337. Cambridge, Massachusetts: Academic Press.

Akyazi, T., Basabe-Desmonts, L., and Benito-Lopez, F. (2018). Review on microfluidic paper-based analytical devices towards commercialisation. *Analytica Chimica Acta*, 1001, 1-17.

Almeida, M. G., Silveira, C. M., and Moura, J. J. G. (2007). Biosensing nitrite using the system nitrite redutase/ Nafion/methyl viologen-A voltammetric study. *Biosensors and Bioelectronics*, 22(11), 2485-2492.

Bihari, P., Vippola, M., Schultes, S., Praetner, M., Khandoga, A. G., Reichel, C. A., Coester, C., Tuomi, T., Rehberg, M., and Krombach, F. (2008). Optimized dispersion of nanoparticles for biological *in vitro* and *in vivo* studies. *Particle and Fibre Toxicology*, 5(1), 14.

Booth, G. (2000). Naphthalene derivatives. In *Ullmann's Encyclopedia of Industrial Chemistry* (Matthias, B., ed.), 6th, pp. 696-711 Weinheim: Wiley-VCH.

Chenier, P. J. (2002). Inorganic nitrogen compounds. In *Survey of Industrial Chemistry* (Philip J. C. ed.), pp. 55-63. Boston, Massachusetts: Springer.

Daniel, W. L., Han, M. S., Lee, J.-S., and Mirkin, C. A. (2009). Colorimetric nitrite and nitrate detection with gold nanoparticle probes and kinetic end points. *Journal of the American Chemical Society*, 131(18), 6362-6363.

Dowsing, R. D., Gibson, J. F., Goodgame, D. M. L., Goodgame, M., and Hayward, P. J. (1968). Determination of the stereochemistry of manganese(II) complexes by electron spin resonance. *Nature*, 219(5158), 1037-1038.

Feiner, G. (2016). Color in cured meat products and fresh meat. In *Salami* (Feiner, G., ed.), pp. 89-101. Cambridge, Massachusetts: Academic Press.

Freitas, C. B., Moreira, R. C., de Oliveira Tavares, M. G., and Coltro, W. K. T. (2016). Monitoring of nitrite, nitrate, chloride and sulfate in environmental samples using electrophoresis microchips coupled with contactless conductivity detection. *Talanta*, 147, 335-341.

Fujimoto, T., Mizukoshi, Y., Nagata, Y., Maeda, Y., and Oshima, R. (2001). Sonolytical preparation of various types of metal nanoparticles in aqueous solution. *Scripta Materialia*, 44(8), 2183-2186.

Hasanzadeh, A., and Hashemzadeh, I. (2021). Microfluidic paper-based devices. In *Biomedical Applications of Microfluidic Devices* (Hamblin, M. R., and Karimi, M. eds.), pp. 257-274. Cambridge, Massachusetts: Academic Press.

Heit, Y. N., Sergentu, D.-C., and Autschbach, J. (2019). Magnetic circular dichroism spectra of transition metal complexes calculated from restricted active space wavefunctions. *Physical Chemistry Chemical Physics*, 21(10), 5586-5597.

Hu, X., Shi, L., Zhang, D., Zhao, X., and Huang, L. (2016). Accelerating the decomposition of $KMnO_4$ by photolysis and auto-catalysis: A green approach to synthesize a layered birnessite-type MnO_2 assembled hierarchical nanostructure. *RSC Advances*, 6(17), 14192-14198.

Jaganyi, D., Altaf, M., and Wekesa, I. (2013). Synthesis and characterization of whisker-shaped MnO_2 nanostructure at room temperature. *Applied Nanoscience*, 3(4), 329-333.

Kim, H., Watthanaphanit, A., and Saito, N. (2016). Synthesis of colloidal MnO_2 with a sheet-like structure by one-pot plasma discharge in permanganate aqueous solution. *RSC Advances*, 6(4), 2826-2834.

Kolb, D. (1988). Oxidation states of manganese. *Journal of Chemical Education*, 65(11), 1004.

Lam, T., Devadhasan, J. P., Howse, R., and Kim, J. (2017). A chemically patterned microfluidic paper-based analytical device (C-μPAD) for point-of-care diagnostics. *Scientific Reports*, 7(1), 1188.

Li, D., He, Q., Yang, Y., Möhwald, H., and Li, J. (2008). Two-stage pH response of poly(4-vinylpyridine) grafted gold nanoparticles. *Macromolecules*, 41(19), 7254-7256.

Li, X., and Harrison, D. J. (1991). Measurement of concentration profiles inside a nitrite ion-selective electrode membrane. *Analytical Chemistry*, 63(19), 2168-2174.

Liu, X., Tang, L., Niessner, R., Ying, Y., and Haisch, C. (2015). Nitrite-triggered surface plasmon-assisted catalytic conversion of *p*-aminothiophenol to *p,p′*-dimercaptoazobenzene on gold nanoparticle: Surface-enhanced raman scattering investigation and potential for nitrite detection. *Analytical Chemistry*, 87(1), 499-506.

Massey, R. C. (1997). Estimation of daily intake of food preservatives. *Food Chemistry*, 60(2), 177-185.

Morakinyo, M. K., Chipinda, I., Hettick, J., Siegel, P. D., Abramson, J., Strongin, R., Martincigh, B. S., and Simoyi, R. H. (2012). Detailed mechanistic investigation into the S-nitrosation of cysteamine. *Canadian Journal of Chemistry*, 9(9), 724-738.

Morbioli, G. G., Mazzu-Nascimento, T., Stockton, A. M., and Carrilho, E. (2017). Technical aspects and challenges of colorimetric detection with microfluidic paper-based analytical devices (μPADs) - A review. *Analytica Chimica Acta*, *970*, 1-22.

Murfin, L. C., López-Alled, C. M., Sedgwick, A. C., Wenk, J., James, T. D., and Lewis, S. E. (2020). A simple, azulene-based colorimetric probe for the detection of nitrite in water. *Frontiers of Chemical Science and Engineering*, 14(1), 90-96.

Murthy, C. P. (2008). *University Chemistry, Volume. II*. New Delhi: New Age International (P) Limited, pp. 13-17.

Porterfield, J. Z., and Zlotnick, A. (2010). A simple and general method for determining the protein and nucleic acid content of viruses by UV absorbance. *Virology*, 407(2), 281-288.

Sakolsatayadorn, P. (2016). Notification of the Ministry of Public Health, Re: Food additive (No.4). The Royal Thai Government Gazette, 133(298). [Online URL: https: //www.ratchakitcha.soc.go.th/DATA/PDF/2559/E/298/3.PDF] accessed on November 3, 2022.

Samatya, S., Kabay, N., Yüksel, Ü., Arda, M., and Yüksel, M. (2006). Removal of nitrate from aqueous solution by nitrate selective ion exchange resins. *Reactive and Functional Polymers*, 66(11), 1206-1214.

Sieben, V. J., Floquet, C. F. A., Ogilvie, I. R. G., Mowlem, M. C., and Morgan, H. (2010). Microfluidic colourimetric chemical analysis system: Application to nitrite detection [10.1039/C002672G]. *Analytical Methods*, 2(5), 484-491.

Singhaphan, P., and Unob, F. (2021). Thread-based platform for nitrite detection based on a modified Griess assay. *Sensors and Actuators B: Chemical*, 327, 128938.

Tomasso, J. R. (1997). Environmental requirements and noninfectious diseases. In *developments in Aquaculture and Fisheries Science* (Harrell, R. M., ed.), pp. 253-270. Amsterdam: Elsevier.

Turdean, G. L., and Szabo, G. (2015). Nitrite detection in meat products samples by square-wave voltammetry at a new single walled carbon naonotubes – myoglobin modified electrode. *Food Chemistry*, 179, 325-330.

Turney, T. A., and Wright, G. A. (1959). Nitrous acid and nitrosation. *Chemical Reviews*, 59(3), 497-513.

Van Eerdenbrugh, B., Alonzo, D. E., and Taylor, L. S. (2011). Influence of particle size on the ultraviolet spectrum of particulate-containing solutions: implications for in-situ concentration monitoring using UV/Vis fiber-optic probes. *Pharmaceutical Research*, 28(7), 1643-1652.

van Faassen, E., Vanin, A. F., and Slama-Schwok, A. (2007). Nitrite as endothelial NO donor under anoxia. In *Radicals for Life* (van Faassen, E., and Vanin, A. F., eds.), pp. 291-312. Amsterdam: Elsevier.

Wang, B., Lin, Z., and Wang, M. (2015). Fabrication of a paper-based microfluidic device to readily determine nitrite ion concentration by simple colorimetric assay. *Journal of Chemical Education*, 92(4), 733-736.

Wang, J., Wong, J. X. H., Kwok, H., Li, X., and Yu, H.-Z. (2016). Facile preparation of nanostructured, superhydrophobic filter paper for efficient water/oil separation. *PLOS ONE*, 11(3), e0151439.

WHO. (2019). *Information Note Nitrosamine impurities. Update on nitrosamine impurities*. [Online URL: https://www.who.int/news/item/20-11-2019-information-note-nitrosamine-impurities] accessed on June 3, 2022.

Yang, L., and Alleman, J. E. (1992). Investigation of batchwise nitrite build-up by an enriched nitrification culture. *Water Science and Technology*, 26(5-6), 997-1005.